

MRFNET: MULTI-RECEPTIVE FIELD NETWORK FOR MULTIVARIATE TIME-SERIES PREDICTION

Anonymous authors

Paper under double-blind review

ABSTRACT

Time series forecasting is a critical topic in machine learning. Although existing deep learning methods have demonstrated outstanding performance and currently dominate this field, the latest state-of-the-art (SOTA) models are increasingly encountering the same limitations: the blockneck of performance. We believe this convergence is due to these models being based on the same mathematical foundations. To address this issue, we draw inspiration from the universal approximation theorem (UAT) and show that most commonly used deep learning models for time series forecasting are specific implementations of UAT. Based on UAT theory and the characteristics of time series data, we propose a new forecasting model called the **Multi-Receptive Field Network (MRFNet)**. This architecture integrates linear, sparse matrix, convolutional, and Fourier transform modules, resulting in an interpretable model with multiple receptive fields that can capture both global and local information. The MRFNet model has been tested extensively on several popular time series forecasting datasets and has achieved superior results.

1 INTRODUCTION

Time series forecasting is a critical problem with widespread applications in areas such as weather forecasting, traffic prediction, stock market analysis, and power consumption forecasting. To tackle this issue, various analytical and statistical methods have been developed. Early research relied on statistical measures like mean and variance to construct models, such as ARMA (McLeod and Li, 1983) and ARIMA (Ho and Xie, 1998; Zhang, 2003). These models have shown impressive accuracy and robustness but have limitations in generalization ability and multivariate time series forecasting.

With the advent of deep learning, a series of deep learning-based time series forecasting models emerged, outperforming traditional machine learning methods. The development of deep learning methods for time series forecasting has largely mirrored the evolution of deep learning models themselves, starting with fully connected neural networks (Kourentzes et al., 2014; Rahman et al., 2015; Torres et al., 2018), followed by recurrent neural networks (RNNs) (Bouktif et al., 2018; Lai et al., 2018; Bahdanau et al., 2014; Hewamalage et al., 2021), and subsequently, convolutional neural networks, Linear model (Zeng et al., 2023), and Transformer networks (Zhou et al., 2021; Wu et al., 2021; Zhou et al., 2022; Nie et al., 2022).

In summary, the three main types of models dominating the time series forecasting field today are linear models, convolutional models, and Transformer models. However, as deep learning continues to evolve, these models have begun to approach a performance bottleneck on widely used public time series forecasting datasets. We believe that the convergence of their performance is due to their shared mathematical foundations. To delve deeper into this issue, we require a fundamental mathematical interpretation of these models. The cornerstone of current deep learning theory is the UAT (Cybenko, 1989). Therefore, our goal is to study time series forecasting networks within the framework of UAT. However, UAT traditionally applies only to perceptron networks, while other forms of networks are more complex and seem to diverge from the theorem. Thus, to investigate complex linear, convolutional, and Transformer models within the UAT framework, we need to express them in a mathematical form consistent with UAT. In UAT2LLMs (Wang and Li, 2024a) and UAT2CVs (Wang and Li, 2024b), the "Matrix-Vector Method" was proposed and used to unify 2D and 3D convolutional, and Transformer-based models within the UAT theoretical framework.

054 Building on these studies, we aim to unify deep learning time series forecasting models within the
055 UAT framework.

056 Through our derivations, we demonstrate that most deep learning models in the time series fore-
057 casting domain, whether used independently or as combinations of the three fundamental modules
058 - Linear, Convolution, and Transformer - are essentially specific implementations of UAT. This
059 explains why they ultimately converge towards similar performance blockneck, as they represent
060 different manifestations of the same mathematical model.

061 Based on UAT theory and the characteristics of time series forecasting problems, we propose
062 the MRFNet model, which integrates linear, 1D convolutional, sparse matrix transformation, and
063 Fourier transform modules. We compare this model with SOTA methods on commonly used time
064 series forecasting datasets and our model achieves SOTA performances on many datasets. Addi-
065 tionally, we performed data preprocessing tailored to the characteristics of time series forecasting
066 data, further enhancing performance. In conclusion, this paper aims to bridge the theoretical gap and
067 practices in time series forecasting. Our goal is to provide researchers and practitioners with tools to
068 understand and advance the theory and practice of time series forecasting. Our main contributions
069 include:

- 071 • We have demonstrated that most of the current deep-learning-based time series prediction
072 models are specific implementations of the UAT, and explained why the current SOTA
073 models converge to similar performance bottlenecks.
- 074 • We proposed the MRFNet model based on the characteristics of time series prediction,
075 which balances both global and local temporal learning. Our model achieved SOTA per-
076 formances across multiple datasets, and we also proved that this model is a specific imple-
077 mentation of UAT for time series prediction.
- 078 • We rearranged the data based on the inherent characteristics of time series data, which
079 further improved the predictive performance of the model.

080 The structure of this paper is organized as follows: Section 2 provides an overview of existing time
081 series forecasting models. In Section 3, we introduce the UAT and the Matrix-Vector Method and
082 discuss their roles in unifying various foundational deep learning modules. In Section 4, we first
083 demonstrate how 1D convolution can be expressed in matrix-vector form using this method, and
084 then present the UAT formulation for general models in time series prediction. Section 5 introduces
085 the MRFNet model (Section 5.1) and describes the time series datasets used (Section 5.2). Section
086 5.3 presents the prediction results of MRFNet and compares them with SOTA models. In Section
087 5.4, we apply feature selection tailored to the characteristics of time series data to further enhance
088 the model’s performance. Finally, in Section 5.5, we provide evidence that current time series
089 forecasting models, being specific implementations of UAT, inevitably converge towards similar
090 performance bottlenecks.

092 2 RELATED WORK

094 **RNN:** Recurrent Neural Networks (RNNs) were very popular for time series forecasting a few years
095 ago, emphasizing the importance of sequence dependencies. RNNs incorporate various gating units
096 to learn connections between different sequence positions (Bouktif et al., 2018; Lai et al., 2018; Bah-
097 danau et al., 2014; Hewamalage et al., 2021). RNNs are fundamentally based on the Markov chain
098 process in mathematics. However, key bottlenecks remain, such as vanishing gradients, substantial
099 training workloads, and rapid error accumulation over longer time spans (Ribeiro et al., 2020).

100 **CNN:** The use of Convolutional Neural Networks (CNNs) for audio-related problems was initially
101 proposed by Oord et al. (2016). Later, Bai et al. (2018) introduced the concept of Temporal Convolu-
102 tional Networks (TCNs) as an alternative for time series forecasting (Bai et al., 2018; Vorbach et al.,
103 2021; Aksan and Hilliges, 2019; Luo and Mesgarani, 2019; Hewage et al., 2020). This approach
104 is influenced by the autoregressive Wavenet model (Oord et al., 2016) and incorporates causal con-
105 volutions to prevent the use of future information. TCNs employ dilated convolutions to capture
106 long-term dependencies in time series data. Several similar models have been developed, including
107 works by Lara-Benítez et al. (2020); Wan et al. (2019); Liu et al. (2021). **The Cross-Period Sparse
Forecasting technique is applied in SparseTSF, which can simplify the forecasting task by decou-**

plung the periodicity and trend in time series data. Dai et al. (2024) propose a novel Periodicity Decoupling Framework (PDF) to capture 2D temporal variations of decoupled series for long-term series forecasting.

Transformer: Transformers have dominated deep learning and shown significant potential in solving time series forecasting problems (Li et al., 2019; Wu et al., 2020; Lim et al., 2021; Wen et al., 2022). The multi-head attention architecture can extract information while positional embeddings help retain sequence position information (Kitaev et al., 2020; Zhang and Zhu, 2018; Wu et al., 2021; Shen and Wang, 2022; Madhusudhanan et al., 2021). However, Transformers are computationally complex, and the setting of hyperparameters greatly influences the performance of Transformer-based models. To address these issues, models like Informer, Autoformer, and Fedformer were developed (Zhou et al., 2021; Wu et al., 2021; Zhou et al., 2022). Liu et al. (2022) tackles time series problems from the perspective of stationarity, while ETSformer (Woo et al., 2022) uses exponential smoothing and frequency attention to replace the self-attention mechanism in Transformers, enhancing accuracy and efficiency. Wang et al. (2023) proposed a Channel Aligned Robust Blend Transformer to address the shortcomings of channel correlation. Additionally, Zhou et al. (2023) explored using pretrained large language models fine-tuned for time series prediction.

Linear: Zeng et al. (2023) argued that Transformers are not the optimal solution for time series forecasting. Instead, they demonstrated that linear methods could achieve SOTA results for both long-range and short-term time series forecasting, outperforming existing models.

3 THE UNIVERSAL APPROXIMATION THEORY

Our objective is to explore time series prediction problems within the framework of the UAT. To begin, we provide a basic introduction to this theorem, originally proposed by Cybenko (1989), which encompasses various conclusions and proofs. In this context, we specifically use the form of the UAT presented in Cybenko (1989) as an illustrative example.

Theorem 2 in Cybenko (1989) asserts that if σ is any continuous sigmoidal function, then finite sums of the form:

$$G(\mathbf{x}) = \sum_{j=1}^N \alpha_j \sigma(\mathbf{W}_j^T \mathbf{x} + \theta_j) \quad (1)$$

are dense in $C(\mathbf{I}_n)$. There are two case for Eq. (1) as follows:

- If $f(\mathbf{x}) \in \mathbb{R}^m$: $G(\mathbf{x}) \in \mathbb{R}^m$, $\mathbf{x} \in \mathbb{R}^n$, $\alpha_i, \mathbf{W}_i \in \mathbb{R}^{(n,m)}$, and $\theta_i \in \mathbb{R}^m$
- If $f(\mathbf{x}) \in \mathbb{R}$: $G(\mathbf{x}) \in \mathbb{R}$, $\mathbf{x} \in \mathbb{R}^n$, $\mathbf{W}_i \in \mathbb{R}^n$, and $\alpha_i, \theta_i \in \mathbb{R}$

\mathbf{x} is the input. For any $f \in C(\mathbf{I}_n)$ and $\varepsilon > 0$, there exists a sum $G(\mathbf{x})$ of the above form for which:

$$|G(\mathbf{x}) - f(\mathbf{x})| < \varepsilon \quad \text{for all } \mathbf{x} \in \mathbf{I}_n. \quad (2)$$

This implies that, for a sufficiently large value of N , a single-layer neural network can approximate any continuous function over a closed interval. Furthermore, Hornik et al. (1989) extends this result, demonstrating that multi-layer feedforward networks also adhere to the UAT, capable of approximating arbitrary Borel measurable functions.

However, the approximate construction of this theorem is not directly applicable to convolutional and Transformer networks, as their basic operations-such as convolution and multi-head attention mechanisms-are difficult to express in the form of matrix-vector multiplication (The basic element in UAT is matrix-vector multiplication: $\alpha_j \sigma(\mathbf{W}_j^T \mathbf{x} + \theta_j)$, where $\mathbf{W}_j^T \mathbf{x}$ can be seen as various modules in networks). Nevertheless, most of the basic solutions for time series problems are based on multi-layer convolutional and Transformer neural networks. These networks involve a series of fundamental operations, such as 1D convolution, multi-head attention, and linear transformations (where the term "linear" differs from the linear transformation in Eq. (1); in Eq. (1), "linear" refers to $\mathbf{W}_j^T \mathbf{x}$ which is a matrix multiplying a vector, while here it refers to a matrix multiplying another matrix). Therefore, if we can rewrite the mathematical expressions of these fundamental operations in the form of a matrix multiplying a vector and prove that they share the same mathematical structure as UAT, it would imply that all conclusions derived from UAT could be applied to multi-layer network architectures composed of these components.

In UAT2LLMs, the Matrix-Vector Method was already used to represent multi-head attention and linear operations in Transformers as a matrix multiplying a vector: $\mathbf{W}\mathbf{x}$. This paper extends the Matrix-Vector Method proposed in UAT2LLMs to prove that 1D convolution can also be expressed in the form of matrix-vector multiplication. The concept behind the matrix-vector method is illustrated in Figure 1. The basic transformation in a network (e.g., 1D convolution) can be understood as $T(\mathbf{W})$, with inputs and outputs represented by \mathbf{x} and \mathbf{y} , respectively. The Matrix-Vector Method transforms the input, output, and the parameters of the operation $T(\mathbf{W})$ within the network into \mathbf{x}' , \mathbf{y}' , and \mathbf{W}' , ensuring that $\mathbf{W}'\mathbf{x}' = \mathbf{y}'$. Note: For convenience, we use the symbol ' to denote the matrix-vector form of the corresponding variable. For example, \mathbf{x} is represented as \mathbf{x}' .

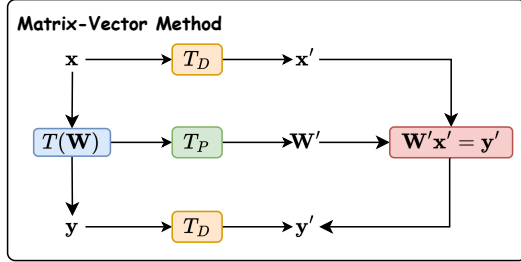


Figure 1: A general description to the Matrix-Vector Method.

4 UNIVERSAL APPROXIMATION THEORY FOR TIME SERIES PREDICTION

Currently, deep learning models for time series forecasting can be summarized as multi-layer networks composed primarily of one or more of the following modules: linear, convolution, and Transformer. These modules are typically connected using residual connections between successive layers. To demonstrate that such multi-layer networks, composed of these basic modules, are concrete implementations of the UAT, we first need to show that these modules can be represented in matrix-vector form. Once this representation is established, we then need to prove that the mathematical form of these networks with residual connections aligns with the UAT equation, Eq. (1).

In UAT2LLMs, it has already been shown that networks composed of multiple Transformer layers have a mathematical form consistent with UAT, and that linear operations can be expressed in matrix-vector form. Therefore, our primary focus here is to prove that 1D convolutional networks can also be represented in matrix-vector form (see Section 4.1). (Note that we will use a special calculation called diamond multiplication: \diamond , and $\mathbf{W} \diamond \mathbf{x} = \mathbf{W}^T \mathbf{x}$. More details could be found in UAT2LLMs) Following that, we demonstrate that the mathematical form of multi-layer networks with residual connections, expressed in matrix-vector terms, is consistent with UAT (see Section 4.2).

4.1 THE MATRIX-VECTOR FORMAT OF 1D CONVOLUTION

In this section, we will transform 1D convolution into the matrix-vector format. Figure 2.Single-channel Output.a vividly illustrates the basic process of single-channel output in 1D convolution: $\mathbf{W} \circledast \mathbf{x} = \mathbf{y}$. Here, the dimension T symbolizes the time size, K is the kernel size, while N represents the feature size. Figure 2.Single-channel Output.b provides a concise example of single-channel output in 1D convolution. Figure 2.Single-channel Output.c further demonstrates how to use the matrix-vector method to transform the convolution of single-channel output into the form of diamond multiplication: $\mathbf{W}' \diamond \mathbf{x}' = \mathbf{y}'$, where \mathbf{x}' , \mathbf{W}' and \mathbf{y}' are generated from \mathbf{x} , \mathbf{W} and \mathbf{y} .

Figure 2.Multi-channel Output.a elaborates on the fundamental process of 1D convolution with multiple convolution kernels and multiple-channel output: $\mathbf{W}_1 \circledast \mathbf{x} = \mathbf{y}_1 \dots \mathbf{W}_O \circledast \mathbf{x} = \mathbf{y}_O$, where the number of output channels O signifies predictions for the next O time steps. Figure 2.Multi-channel Output.b offers a simplified example of Figure 2.Multi-channel Output.a, and Figure 2.Multi-channel Output.c employs the matrix-vector method to convert the convolution of multiple-channel output into the form of diamond multiplication: $\mathbf{W}' \diamond \mathbf{x} = \mathbf{y}'$, where \mathbf{W}' is generated from $\mathbf{W}_1 \dots \mathbf{W}_O$ and \mathbf{y}' is generated from $\mathbf{y}_1 \dots \mathbf{y}_O$. With the relationship between diamond multiplication and matrix

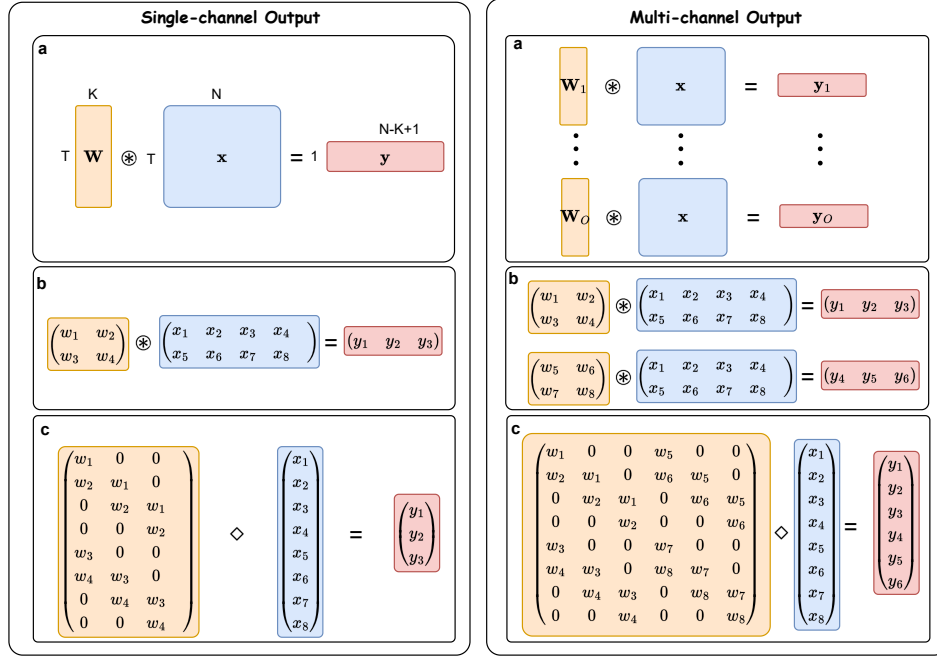


Figure 2: Illustration on how 1D convolution can be represented in matrix-vector form. The left side corresponds to a 1D convolution with a single output channel, while the right side represents a 1D convolution with multiple output channels. The convolution kernel, input data, and output data are indicated by orange, blue, and pink boxes, respectively. (a) Conceptual diagram of a 1D convolution, using different colored boxes to represent data and parameters. (b) A simple example of a 1D convolution. (c) The matrix-vector representation for the 1D convolution in (b).

multiplication, we can derive the following formula:

$$\mathbf{x}_{i+1} = \mathbf{W}_i \circledast \mathbf{x}_i \rightarrow (\mathbf{x}^{i+1})' = \mathbf{W}'_i \diamond \mathbf{x}'_i = (\mathbf{W}'_i)^T \mathbf{x}'_i \quad (3)$$

Here, $\mathbf{x}_i \in \mathbb{R}^{(N,M)}$ represents the input of the i -th layer, while $\mathbf{x}_{i+1} \in \mathbb{R}^{(O,M-k+1)}$ is the output from the same layer. The matrix $\mathbf{W}_i \in \mathbb{R}^{(O,N,K)}$ are convolution kernel with the kernel size is K and the number of kernel is O . \mathbf{x}'_{i+1} , \mathbf{x}'_i , \mathbf{W}'_i are transformed from $\mathbf{x}_{i+1} \in \mathbb{R}^{(O(M-k+1),1)}$, $\mathbf{x}_i \in \mathbb{R}^{(NM,1)}$, $\mathbf{W}_i \in \mathbb{R}^{(NM,O(M-k+1))}$ based on matrix-vector method.

So we have proved the 1D convolution in time series can be represented in matrix-vector format. In the context of time series prediction, we observe that a single operation of 1D convolution learns the correlations among K features at all time points using the convolution kernel. It generates output for a single feature at a specific time step. Sliding the convolution kernel can produce output for multiple features at the same time step, and increasing the number of convolution kernels enables obtaining outputs for multiple features across multiple time steps.

4.2 THE UAT FORMAT OF DEEP LEARNING NETWORKS IN TIME SERIES PREDICTION

Currently, the main deep learning networks used in time series forecasting are based on linear, convolutional and Transformer modules, which are typically connected in a residual form. So our purpose is to prove that the mathematical format of residual-based networks is consistent with UAT. It has already been proven in UAT2LLMs that the mathematical form of multi-layer Transformer networks is consistent with that of UAT, which can be written as:

$$\mathbf{x}_{i+1} = (\mathbf{W}'_{i+1,1} \mathbf{x}_0 + \mathbf{b}_{i+1,1}) + \sum_{j=1}^{i+1} \mathbf{W}'_{j,3} \sigma(\mathbf{W}'_{j,2} \mathbf{x}'_0 + \mathbf{b}'_{j,2}) \quad (4)$$

where \mathbf{x}_{i+1} is the output of $i+1$ -th layer, \mathbf{x}_0 is the input of the network, $\mathbf{b}'_{j,2} = (\mathbf{W}'_{j,2} \mathbf{b}'_{j-1,3} + \mathbf{b}'_{j,2}) + \mathbf{W}'_{j,2} \text{UAT}_{j-1}^R$, where $\text{UAT}_{j-1}^R = \sum_{k=1}^{j-1} \mathbf{W}'_{k,3} \sigma(\mathbf{W}'_{k,2} \mathbf{x}'_0 + \mathbf{b}'_{k,2})$. The term $\mathbf{b}'_{j,2}$ is approx-

270
271
272
273
274
275
276
277
278
279
280
281
282
283
284
285
286
287
288
289
290
291
292
293
294
295
296
297
298
299
300
301
302
303
304
305
306
307
308
309
310
311
312
313
314
315
316
317
318
319
320
321
322
323

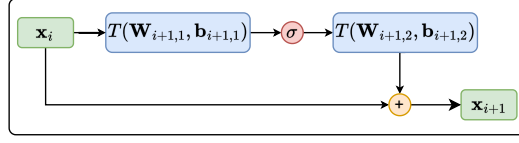


Figure 3: A general description of the residual-based module in a network.

imated by the j layer of UAT with \mathbf{x}_0 as input. This enhances the model’s ability to dynamically adjust functions based on input.

Here, we aim to prove that the mathematical form of residual-based multi-layer 1D convolutional and Linear networks is also consistent with UAT. Given the diversity of network architectures, we assume, without loss of generality, that the network structure is as depicted in Figure 3.

In this structure, T represents either a linear or a convolution, while \mathbf{W}_i and \mathbf{b}_i denote the corresponding parameters. The mathematical representation of the network shown in Figure 3 can then be expressed as follows:

$$\mathbf{x}_{i+1} = \mathbf{x}_i + T_{i+1}\{\sigma[T_i(\mathbf{x}_i)]\} \quad (5)$$

Since we have demonstrated that 1D convolution can be expressed in the form of matrix-vector multiplication, and UAT2LLMs has shown that linear operations can also be expressed as matrix-vector multiplication, Eq. (5) can therefore be rewritten as:

$$\begin{aligned} \mathbf{x}'_{i+1} &= \mathbf{x}'_i + \mathbf{W}'_{i+1,2}\sigma(\mathbf{W}'_{i+1,1}\mathbf{x}'_i + \mathbf{b}'_{i+1,1}) + \mathbf{b}'_{i+1,2} \\ &= (\mathbf{x}'_i + \mathbf{b}'_{i+1,2}) + \mathbf{W}'_{i+1,2}\sigma(\mathbf{W}'_{i+1,1}\mathbf{x}'_i + \mathbf{b}'_{i+1,1}) \end{aligned} \quad (6)$$

Eq. (6) is mathematically identical to the residual-based convolutional neural networks in UAT2CVs. UAT2CVs has already demonstrated that the mathematical form of a multi-layer network, as expressed in Eq. (6), is mathematically consistent with UAT, which is given by:

$$\mathbf{x}'_{i+1} = (\mathbf{x}'_0 + \mathbf{b}'_{i+1,2}) + \sum_{j=1}^{i+1} \mathbf{W}'_{j,2}\sigma(\mathbf{W}'_{j,1}\mathbf{x}'_0 + \mathbf{b}'_{j,1}) \quad (7)$$

where $\mathbf{b}'_{j,1} = (\mathbf{W}'_{j,1}\mathbf{b}'_{j-1,2} + \mathbf{b}'_{j,1}) + \mathbf{W}'_{j,1}UAT_{j-1}^R$ and $UAT_{j-1}^R = \sum_{k=1}^{j-1} \mathbf{W}'_{k,2}\sigma(\mathbf{W}'_{k,1}\mathbf{x}'_0 + \mathbf{b}'_{k,1})$. Eq. (7) conforming to the UAT form given in Eq. (1). In this equation, $\mathbf{b}_{j,1}$ is a dynamic parameter approximated by j layers UAT ($j > 1$).

According to the above derivation, we know most deep-learning neural networks are the implementations of UAT.

5 MRFNET AND EXPERIMENTS

In this section, we first introduce the MRFNet architecture and discuss its key features (Section 5.1). Next, we describe the datasets used in our study (Section 5.2) and compare the performances of our model with several current SOTA models to demonstrate its effectiveness (Section 5.4). Following this, we leverage the characteristics of time series data to further enhance the model’s performances (Section 5.4). Finally, in Section 5.5, we use experiments to validate that these UAT-based models ultimately converge to the same performance bottleneck.

5.1 MRFNET

Based on the characteristics of time series data, we designed the MRFNet model for time series forecasting. The architecture of MRFNet is illustrated in Figure 4: first, a linear module is used to embed time information. In time series forecasting, the changes in the sequence are often influenced by natural factors, such as seasonality and periodicity. Therefore, it is necessary to embed time

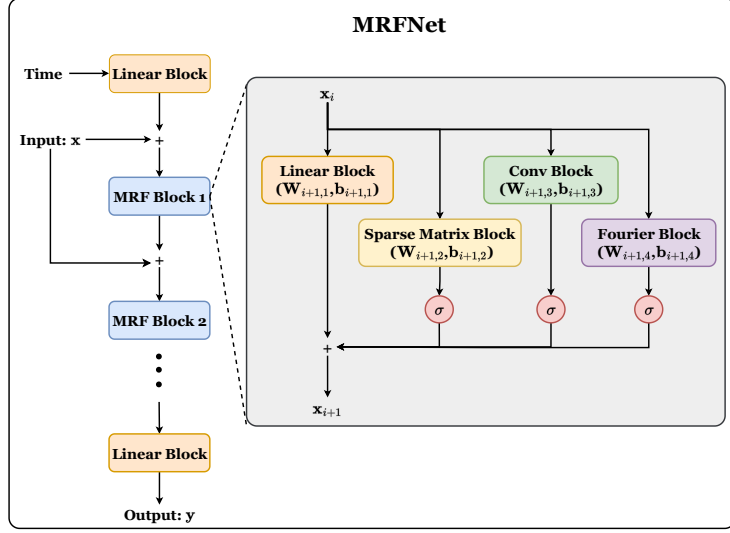


Figure 4: Overview of the MRFNet model’s architecture. The details of the MRF block are shown on the right side.

information. The model then leverages multiple MRF modules for learning, and finally, a Linear block is applied to produce the output.

The MRF module consists of four main components: the Linear Block, Sparse Matrix Block, Conv Block, and Fourier Block. The Linear Block, which can be represented as $\mathbf{W}_{i+1,1}\mathbf{x} + \mathbf{b}_{i+1,1}$, performs linear transformations on the input data, capturing the overall temporal trends within the data. Given that features often share common attributes, we introduce a Linear Block to learn these shared characteristics, aiming to capture the intrinsic commonalities within the data. The Sparse Matrix Block focuses on learning local temporal features, which can be represented as $(\mathbf{W}_S \odot \mathbf{W}_{i+1,2})\mathbf{x} + \mathbf{b}_{i+1,2}$. Where \mathbf{W}_S is a custom sparse matrix composed of 0s and 1s, ensuring the sparsity of $\mathbf{W}_{i+1,2}$.

The Conv Block employs 1D convolution, commonly used in time series forecasting, allowing the model to learn multi-feature correlations based on the size of the convolution kernel, represented as: $\mathbf{W}_{i+1,3} \otimes \mathbf{x}_i + \mathbf{b}_{i+1,3}$. The connection between convolution and the Fourier Block can be expressed as $\mathbf{x} \otimes \mathbf{h} = \mathbf{F}^{-1}[\mathbf{F}\mathbf{x} \odot \mathbf{F}\mathbf{h}]$. In the frequency domain, we have the capacity to learn \mathbf{h} , which is equivalent to $\mathbf{x} \otimes \mathbf{h} = \mathbf{F}^{-1}\mathbf{W}\mathbf{F}\mathbf{x}$. Thus, we introduce an enhanced convolutional variant in the neural network, $\mathbf{F}^{-1}\mathbf{W}\mathbf{F}\mathbf{x}$. This enables us to extract features in the frequency domain and achieve a broader receptive field, as demonstrated in the [Appendix D](#). Additionally, the Fourier Transform is known for its ability to generate sparse representations, where only a few coefficients contain significant information, which can be used to emphasize key features.

Since we have proven that both linear transformations and convolutions can be expressed in a matrix-vector format, all four basic modules within the MRF Block can also be represented in this format. The Sparse Matrix Block can be considered a special type of linear transformation, while the Fourier Block can also be treated as a special case of linear transformation because \mathbf{F}^{-1} and \mathbf{F} are fixed. Therefore, we can define $\mathbf{W}_F = \mathbf{F}^{-1}\mathbf{W}\mathbf{F}$, which allows the Fourier Block to be viewed as a special Linear transformation. Consequently, the general form of MRFNet can be expressed as:

$$\begin{aligned} \mathbf{x}'_{i+1} = & \mathbf{W}'_{i+1,1}\mathbf{x}'_i + \mathbf{b}'_{i+1,1} + \sigma(\mathbf{W}'_{i+1,2}\mathbf{x}'_i + \mathbf{b}'_{i+1,2}) \\ & + \sigma(\mathbf{W}'_{i+1,3}\mathbf{x}'_i + \mathbf{b}'_{i+1,3}) + \sigma(\mathbf{W}'_{i+1,4}\mathbf{x}'_i + \mathbf{b}'_{i+1,4}) \end{aligned} \quad (8)$$

Based on Eq. (8), it is easy to prove that MRFNet is also an implementation of UAT and effectively increases the depth of the UAT. We provide the proof in [Appendix B](#). The various transformations within the MRF module can all be represented as corresponding matrix-vector multiplications, differing only in the size of the learned receptive field. By efficiently handling different temporal

Table 1: A general description of all datasets.

Datasets	ETTh1&ETTh2	ETTh1 &ETTh2	Traffic	Electricity	Weather	ILI
Variates	7	7	862	321	21	7
Timesteps	17,420	69,680	17,544	26,304	52,696	966
Granularity	1hour	5min	1hour	1hour	10min	1week

Table 2: Multivariate predictions of ETTh1, ETTh2, ETTm1, ETTm2, Traffic, Electricity, Weather and ILI, by twelve models. The best results are highlighted in bold red. The second-best results are indicated with highlighted in bold black. Here, we provide a comparison of only some models. A more comprehensive comparison is presented in Table 5 in the Appendix.

Methods	Metric	MRFNet		GPT2(6)		DLinear		PatchTST		TimesNet		FEDformer		Autoformer	
		MSE	MAE	MSE	MAE	MSE	MAE	MSE	MAE	MSE	MAE	MSE	MAE	MSE	MAE
Weather	96	0.149	0.191	0.162	0.212	0.176	0.237	0.149	0.198	0.172	0.220	0.217	0.296	0.266	0.336
	192	0.193	0.235	0.204	0.248	0.220	0.282	0.194	0.241	0.219	0.261	0.276	0.336	0.307	0.367
	336	0.245	0.278	0.254	0.286	0.265	0.319	0.245	0.282	0.280	0.306	0.339	0.380	0.359	0.395
	720	0.315	0.329	0.326	0.337	0.333	0.362	0.314	0.334	0.365	0.359	0.403	0.428	0.419	0.428
	Avg	0.225	0.258	0.237	0.270	0.248	0.300	0.225	0.264	0.259	0.287	0.309	0.360	0.338	0.382
ETTh1	96	0.364	0.393	0.376	0.397	0.375	0.399	0.370	0.399	0.384	0.402	0.376	0.419	0.449	0.459
	192	0.402	0.415	0.416	0.418	0.405	0.416	0.413	0.421	0.436	0.429	0.420	0.448	0.500	0.482
	336	0.442	0.444	0.442	0.433	0.439	0.443	0.422	0.436	0.491	0.469	0.459	0.465	0.521	0.496
	720	0.434	0.454	0.477	0.456	0.472	0.490	0.447	0.466	0.521	0.500	0.506	0.507	0.514	0.512
	Avg	0.410	0.426	0.427	0.426	0.422	0.437	0.413	0.430	0.458	0.450	0.440	0.460	0.496	0.487
ETTh2	96	0.273	0.330	0.285	0.342	0.289	0.353	0.274	0.336	0.340	0.374	0.358	0.397	0.346	0.388
	192	0.341	0.376	0.354	0.389	0.383	0.418	0.339	0.379	0.402	0.414	0.429	0.439	0.456	0.452
	336	0.366	0.396	0.373	0.407	0.448	0.465	0.329	0.380	0.452	0.452	0.496	0.487	0.482	0.486
	720	0.385	0.423	0.406	0.441	0.605	0.551	0.379	0.422	0.462	0.468	0.463	0.474	0.515	0.511
	Avg	0.341	0.381	0.354	0.394	0.431	0.446	0.330	0.379	0.414	0.427	0.437	0.449	0.450	0.459
ETTh1	96	0.297	0.342	0.292	0.346	0.299	0.343	0.290	0.342	0.338	0.375	0.379	0.419	0.505	0.475
	192	0.334	0.366	0.332	0.372	0.335	0.365	0.332	0.369	0.374	0.387	0.426	0.441	0.553	0.496
	336	0.366	0.385	0.366	0.394	0.369	0.386	0.366	0.392	0.410	0.411	0.445	0.459	0.621	0.537
	720	0.407	0.411	0.417	0.421	0.425	0.421	0.416	0.420	0.478	0.450	0.543	0.490	0.671	0.561
	Avg	0.351	0.376	0.352	0.383	0.357	0.378	0.351	0.380	0.400	0.406	0.448	0.452	0.588	0.517
ETTh2	96	0.163	0.246	0.173	0.262	0.167	0.269	0.165	0.255	0.187	0.267	0.203	0.287	0.255	0.339
	192	0.219	0.287	0.229	0.301	0.224	0.303	0.220	0.292	0.249	0.309	0.269	0.328	0.281	0.340
	336	0.275	0.323	0.286	0.341	0.281	0.342	0.274	0.329	0.321	0.351	0.325	0.366	0.339	0.372
	720	0.354	0.377	0.378	0.401	0.397	0.421	0.362	0.385	0.408	0.403	0.421	0.415	0.433	0.432
	Avg	0.252	0.333	0.266	0.326	0.267	0.333	0.255	0.315	0.291	0.333	0.305	0.349	0.327	0.371
ILI	24	1.757	0.857	2.063	0.881	2.215	1.081	1.319	0.754	2.317	0.934	3.228	1.260	3.483	1.287
	36	2.085	0.915	1.868	0.892	1.963	0.963	1.430	0.834	1.972	0.920	2.679	1.080	3.103	1.148
	48	1.972	0.899	1.790	0.884	2.130	1.024	1.553	0.815	2.238	0.940	2.622	1.078	2.669	1.085
	60	1.998	0.923	1.979	0.957	2.368	1.096	1.470	0.788	2.027	0.928	2.857	1.157	2.770	1.125
	Avg	1.953	0.898	1.925	0.903	2.169	1.041	1.443	0.797	2.139	0.931	2.847	1.144	3.006	1.161
ECL	96	0.127	0.218	0.139	0.238	0.140	0.237	0.129	0.222	0.168	0.272	0.193	0.308	0.201	0.317
	192	0.144	0.234	0.153	0.251	0.153	0.249	0.157	0.240	0.184	0.289	0.201	0.315	0.222	0.334
	336	0.159	0.251	0.169	0.266	0.169	0.267	0.163	0.259	0.198	0.300	0.214	0.329	0.231	0.338
	720	0.192	0.280	0.206	0.297	0.203	0.301	0.197	0.290	0.220	0.320	0.246	0.355	0.254	0.361
	Avg	0.155	0.245	0.167	0.263	0.166	0.263	0.161	0.252	0.192	0.295	0.214	0.327	0.227	0.338
Traffic	96	0.386	0.241	0.388	0.282	0.410	0.282	0.360	0.249	0.593	0.321	0.587	0.366	0.613	0.388
	192	0.399	0.248	0.407	0.290	0.423	0.287	0.379	0.256	0.617	0.336	0.604	0.373	0.616	0.382
	336	0.414	0.274	0.412	0.294	0.436	0.296	0.392	0.264	0.629	0.336	0.621	0.383	0.622	0.337
	720	0.457	0.277	0.450	0.312	0.466	0.315	0.432	0.286	0.640	0.350	0.626	0.382	0.660	0.408
	Avg	0.414	0.260	0.414	0.294	0.433	0.295	0.390	0.263	0.620	0.336	0.610	0.376	0.628	0.379

components and adjusting the receptive field, the model can capture subtle variations in the data. The overall time complexity of the model is $O(L \cdot T^2 \cdot C \cdot K)$, where L , T , C , and K represent the number of network layers, the temporal dimension, the feature dimension, and the convolution kernel size, respectively.

5.2 DATASETS

The experiments were conducted on real-world datasets (Zhou et al., 2021), including (1) Electricity Transformer Temperature (ETT), (2) Electricity, and (3) Traffic, (4) Weather, (5) ILI. The details of all datasets can be found in (Wu et al., 2021). The data source is available at github¹. It should be noted that ETT consists of four different datasets: ETTh1, ETTh2, ETTm1, and ETTm2, each of which has seven variables. We evaluate our model using Mean Absolute Errors (MAE) and Mean

¹<https://github.com/thuml/Autoformer>

Squared Errors (MSE), as used in (Zhou et al., 2021). Smaller values of MAE/MSE indicate better model performance. We use the average values for all predictions. The details of all datasets are shown in Table 1. In Appendix A, we give the data setting for training, evaluation and testing.

5.3 RESULTS OF MRFNET

In Table 2, we compare our model with the current SOTA models for time series prediction. Our model demonstrates superior performances on these datasets, achieving SOTA results in most cases (except for the ILI dataset, which is primarily affected by the characteristics of the data itself; we will provide a solution for this issue in Section 5.4). However, when analyzing the results across all models, it becomes evident that the current SOTA models - MRFNet, GPT2(6) (Zhou et al., 2023), DLinear (Zeng et al., 2023), and PatchTST (Nie et al., 2022) - converge towards a similar performance bottleneck. This is because they are all composed of multi-layer Transformers and Linear components, which we have proven to be specific implementations of the dynamic UAT, leading them to the same blockneck with limited data. Additional results for univariate prediction can be found in Appendix F.

Although the MRFNet proposed in this paper is specifically designed to leverage the characteristics of temporal data, it remains categorized within the UAT function framework. Consequently, MRFNet provides only limited improvements over previous prediction results. However, experimental outcomes demonstrate that the model achieves SOTA performance, thereby validating its effectiveness. We believe that another critical factor contributing to the existing performance bottleneck lies in the inherent limitations of the data itself. To address this, in Section 5.4, we conducted more in-depth data processing and training optimizations tailored to the unique properties of temporal data.

5.4 DATA EFFECTS

In this section, we will solve the bottleneck problem from the perspective of data. A crucial characteristic of time series data is its periodicity. However, this periodicity may change over time due to external factors (e.g., advancements in science leading to a gradual increase in electricity demand). This gives data a specific property: data points closer to the prediction point have a greater impact on the results (e.g., when forecasting electricity demand for 2024, the data from 2023 is more relevant, while earlier years are less so).

Leveraging this property, we designated the beginning part of the ETT data as the validation set, kept the test set unchanged, and used the remaining data for training. The results, as shown in Table 3 for MRFNet*. As seen in Table 3, the results improved substantially after adjusting the allocation of the training and validation sets.

Another issue is the relatively poor performance of MRFNet on the ILI dataset. We believe this is primarily due to the nature of the data itself. Not all features in the ILI dataset are correlated (see Appendix C) and forcing all data to be trained together may lead to worse results. Based on the characteristics of the ILI data, we divided it into two groups and trained them separately. The results are shown in Table 4. For more details, please refer to the Appendix C.

5.5 ABLATION EXPERIMENT

We decompose the MRFNet model into three variants: LS (Linear-Sparse Matrix), LC (Linear-Convolution), and LF (Linear-Fourier Transform), and compare them against the full MRFNet

Table 3: We re-divided the training and validation sets for the ETTh1, ETTh2, ETTm1, and ETTm2 datasets, then retrained the models. The test results were obtained on the same test sets.

Models		MRFNet		MRFNet*		PatchTST/64	
Metric		MSE	MAE	MSE	MAE	MSE	MAE
ETTh1	96	0.364	0.393	0.302	0.368	0.370	0.400
	192	0.402	0.415	0.343	0.397	0.413	0.429
	336	0.442	0.444	0.366	0.415	0.422	0.440
	720	0.434	0.454	0.387	0.446	0.447	0.468
ETTh2	96	0.273	0.330	0.246	0.319	0.274	0.337
	192	0.341	0.376	0.308	0.359	0.341	0.382
	336	0.366	0.396	0.325	0.381	0.329	0.384
	720	0.385	0.423	0.353	0.408	0.379	0.422
ETTm1	96	0.297	0.342	0.243	0.316	0.293	0.346
	192	0.334	0.366	0.280	0.342	0.333	0.370
	336	0.360	0.385	0.299	0.359	0.369	0.392
	720	0.407	0.411	0.353	0.396	0.416	0.420
ETTm2	96	0.163	0.246	0.144	0.233	0.166	0.256
	192	0.219	0.287	0.197	0.273	0.223	0.296
	336	0.275	0.323	0.245	0.309	0.274	0.329
	720	0.354	0.377	0.306	0.357	0.362	0.385

Table 4: We split the 7 features of the ILI dataset into two groups for separate training and prediction. The seven features are labeled as Class 1 to Class 7. Group 1: Class 1, 2, 3, 4, 5; Group 2: Class 6,7. Ori: Results from training with all features together. Split: Results from training after splitting the features into two groups.

Methods	Class 1		Class 2		Class 3		Class 4		Class 5		Class 6		Class 7		
	MSE	MAE	MSE	MAE	MSE	MAE	MSE	MAE	MSE	MAE	MSE	MAE	MSE	MAE	
Ori	Avg	0.581	0.860	0.630	1.046	1.139	2.821	1.020	2.807	1.269	4.236	0.744	0.800	0.904	1.097
Split	Avg	0.366	0.233	0.339	0.220	0.294	0.160	0.304	0.199	0.367	0.254	0.188	0.103	0.184	0.094

model. Table 5 presents the results of our ablation study. The results indicate that while certain models perform less well on specific datasets, such as the LC model on the Weather dataset, their overall performance remains very close. Notably, the MRFNet model consistently ranks either best or second-best across all datasets.

Table 5: Ablation Experiment on of ETTh1, ETTm2, and Weather. The best results are highlighted in bold red. The second-best results are indicated with an underlined orange line. The best results are highlighted in bold red. The second-best results are indicated with an underlined orange line

Models	MRFNet		LS		LC		LF		
	MSE	MAE	MSE	MAE	MSE	MAE	MSE	MAE	
ETTh1	96	0.149	0.191	0.170	0.208	0.169	0.208	0.148	0.189
	192	0.193	0.235	0.211	0.249	0.212	0.248	0.193	0.235
	336	0.245	0.278	0.257	0.286	0.257	0.286	0.244	0.277
	720	0.315	0.329	0.321	0.335	0.322	0.336	0.312	0.326
ETTh2	96	0.297	0.342	0.297	0.341	0.275	0.343	0.296	0.341
	192	0.334	0.366	0.337	0.365	0.335	0.365	0.336	0.368
	336	0.360	0.385	0.370	0.388	0.369	0.386	0.357	0.383
	720	0.407	0.411	0.421	0.415	0.425	0.421	0.409	0.413
ETTh2	96	0.163	0.246	0.160	0.245	0.161	0.246	0.161	0.245
	192	0.219	0.287	0.215	0.284	0.215	0.284	0.221	0.286
	336	0.275	0.323	0.267	0.321	0.268	0.330	0.277	0.324
	720	0.354	0.377	0.354	0.375	0.352	0.375	0.362	0.380

These results support our conclusions: first, we have demonstrated that these models inherently share the same mathematical properties, which explains the similarity in their results. Second, MRFNet is equivalent to an increased network depth compared to the other models and benefits from its more comprehensive feature learning. As a result, MRFNet maintains SOTA performance or near-SOTA performance across all datasets, further validating its robustness and superiority.

Additionally, in Appendix E, we compare the weights of MRFNet, LS, LC, and LF at the same layer. The weights for the same dataset exhibit similar textures, suggesting that, in general, they are learning similar information patterns. Given that we have proven these models share the same mathematical framework, the primary differences lie in the size of their receptive fields, with each model’s module playing a similar role. However, due to the different receptive field sizes, the specific patterns they learn may vary slightly, though the overall trend remains consistent.

6 CONCLUSION

In this paper, we demonstrate that most models in the field of time series forecasting are specific implementations of the UAT, which explains why current SOTA models in time series forecasting tend to converge towards the same performance bottleneck. Based on the principles of UAT and the characteristics of time series data, we have designed a new model, MRFNet, for time series prediction. MRFNet integrates linear modules, sparse matrix modules, convolutional modules, and Fourier transform modules, effectively capturing both global and local receptive field information. Through extensive testing on various common datasets, the MRFNet model has demonstrated its superiority, achieving SOTA-level performance. Additionally, by leveraging the intrinsic properties of time series data, we further refined the data, significantly enhancing the performance on certain datasets. Finally, we conducted experiments to confirm that time series forecasting models based on UAT theory eventually converge to a similar performance bottleneck. **In the future, we will further try to tackle the challenges of bottleneck from the perspective of UAT and data.**

REFERENCES

- 540
541
542 A. I. McLeod and W. K. Li, “Diagnostic checking arma time series models using squared-residual
543 autocorrelations,” *Journal of time series analysis*, vol. 4, no. 4, pp. 269–273, 1983.
- 544
545 S. L. Ho and M. Xie, “The use of arima models for reliability forecasting and analysis,” *Computers
546 & industrial engineering*, vol. 35, no. 1-2, pp. 213–216, 1998.
- 547
548 G. P. Zhang, “Time series forecasting using a hybrid arima and neural network model,” *Neurocom-
549 puting*, vol. 50, pp. 159–175, 2003.
- 550
551 N. Kourentzes, D. K. Barrow, and S. F. Crone, “Neural network ensemble operators for time series
552 forecasting,” *Expert Systems with Applications*, vol. 41, no. 9, pp. 4235–4244, 2014.
- 553
554 M. M. Rahman, M. M. Islam, K. Murase, and X. Yao, “Layered ensemble architecture for time
555 series forecasting,” *IEEE transactions on cybernetics*, vol. 46, no. 1, pp. 270–283, 2015.
- 556
557 J. F. Torres, A. Galicia, A. Troncoso, and F. Martínez-Álvarez, “A scalable approach based on deep
558 learning for big data time series forecasting,” *Integrated Computer-Aided Engineering*, vol. 25,
559 no. 4, pp. 335–348, 2018.
- 560
561 S. Bouktif, A. Fiaz, A. Ouni, and M. A. Serhani, “Optimal deep learning lstm model for electric load
562 forecasting using feature selection and genetic algorithm: Comparison with machine learning
563 approaches,” *Energies*, vol. 11, no. 7, p. 1636, 2018.
- 564
565 G. Lai, W.-C. Chang, Y. Yang, and H. Liu, “Modeling long-and short-term temporal patterns with
566 deep neural networks,” in *The 41st International ACM SIGIR Conference on Research & Devel-
567 opment in Information Retrieval*, 2018, pp. 95–104.
- 568
569 D. Bahdanau, K. Cho, and Y. Bengio, “Neural machine translation by jointly learning
570 to align and translate,” *CoRR*, vol. abs/1409.0473, 2014. [Online]. Available: <https://api.semanticscholar.org/CorpusID:11212020>
- 571
572 H. Hewamalage, C. Bergmeir, and K. Bandara, “Recurrent neural networks for time series forecast-
573 ing: Current status and future directions,” *International Journal of Forecasting*, vol. 37, no. 1, pp.
574 388–427, 2021.
- 575
576 A. Zeng, M. Chen, L. Zhang, and Q. Xu, “Are transformers effective for time series forecasting?”
577 in *Proceedings of the AAAI conference on artificial intelligence*, vol. 37, no. 9, 2023, pp. 11 121–
578 11 128.
- 579
580 H. Zhou, S. Zhang, J. Peng, S. Zhang, J. Li, H. Xiong, and W. Zhang, “Informer: Beyond efficient
581 transformer for long sequence time-series forecasting,” in *Proceedings of the AAAI conference on
582 artificial intelligence*, vol. 35, no. 12, 2021, pp. 11 106–11 115.
- 583
584 H. Wu, J. Xu, J. Wang, and M. Long, “Autoformer: Decomposition transformers with auto-
585 correlation for long-term series forecasting,” *Advances in Neural Information Processing Systems*,
586 vol. 34, pp. 22 419–22 430, 2021.
- 587
588 T. Zhou, Z. Ma, Q. Wen, X. Wang, L. Sun, and R. Jin, “Fedformer: Frequency enhanced decomposed
589 transformer for long-term series forecasting,” in *International Conference on Machine Learning*.
590 PMLR, 2022, pp. 27 268–27 286.
- 591
592 Y. Nie, N. H. Nguyen, P. Sinthong, and J. Kalagnanam, “A time series is worth 64 words: Long-term
593 forecasting with transformers,” *arXiv preprint arXiv:2211.14730*, 2022.
- 588
589 G. V. Cybenko, “Approximation by superpositions of a sigmoidal function,” *Mathematics
590 of Control, Signals and Systems*, vol. 2, pp. 303–314, 1989. [Online]. Available:
591 <https://api.semanticscholar.org/CorpusID:3958369>
- 592
593 W. Wang and Q. Li, “Universal approximation theory: The basic theory for transformer-based
large language models,” 2024. [Online]. Available: <https://api.semanticscholar.org/CorpusID:271902755>

- 594 —, “Universal approximation theory: The basic theory for deep learning-based computer vision
595 models,” *ArXiv*, vol. abs/2407.17480, 2024. [Online]. Available: [https://api.semanticscholar.org/
596 CorpusID:271432349](https://api.semanticscholar.org/CorpusID:271432349)
597
- 598 A. H. Ribeiro, K. Tiels, L. A. Aguirre, and T. Schön, “Beyond exploding and vanishing gradients:
599 analysing rnn training using attractors and smoothness,” in *International conference on artificial
600 intelligence and statistics*. PMLR, 2020, pp. 2370–2380.
- 601 A. v. d. Oord, S. Dieleman, H. Zen, K. Simonyan, O. Vinyals, A. Graves, N. Kalchbrenner,
602 A. Senior, and K. Kavukcuoglu, “Wavenet: A generative model for raw audio,” *arXiv preprint
603 arXiv:1609.03499*, 2016.
- 604 S. Bai, J. Z. Kolter, and V. Koltun, “An empirical evaluation of generic convolutional and recurrent
605 networks for sequence modeling,” *arXiv preprint arXiv:1803.01271*, 2018.
- 606 C. Vorbach, R. Hasani, A. Amini, M. Lechner, and D. Rus, “Causal navigation by continuous-
607 time neural networks,” *Advances in Neural Information Processing Systems*, vol. 34, pp. 12 425–
608 12 440, 2021.
- 609 E. Aksan and O. Hilliges, “Stcn: Stochastic temporal convolutional networks,” *arXiv preprint
610 arXiv:1902.06568*, 2019.
- 611 Y. Luo and N. Mesgarani, “Conv-tasnet: Surpassing ideal time–frequency magnitude masking for
612 speech separation,” *IEEE/ACM transactions on audio, speech, and language processing*, vol. 27,
613 no. 8, pp. 1256–1266, 2019.
- 614 P. Hewage, A. Behera, M. Trovati, E. Pereira, M. Ghahremani, F. Palmieri, and Y. Liu, “Temporal
615 convolutional neural (tcn) network for an effective weather forecasting using time-series data from
616 the local weather station,” *Soft Computing*, vol. 24, no. 21, pp. 16 453–16 482, 2020.
- 617 P. Lara-Benítez, M. Carranza-García, J. M. Luna-Romera, and J. C. Riquelme, “Temporal convolu-
618 tional networks applied to energy-related time series forecasting,” *applied sciences*, vol. 10, no. 7,
619 p. 2322, 2020.
- 620 R. Wan, S. Mei, J. Wang, M. Liu, and F. Yang, “Multivariate temporal convolutional network: A
621 deep neural networks approach for multivariate time series forecasting,” *Electronics*, vol. 8, no. 8,
622 p. 876, 2019.
- 623 M. Liu, A. Zeng, Z. Xu, Q. Lai, and Q. Xu, “Time series is a special sequence: Forecasting with
624 sample convolution and interaction,” *arXiv preprint arXiv:2106.09305*, vol. 1, no. 9, 2021.
- 625 T. Dai, B. Wu, P. Liu, N. Li, J. Bao, Y. Jiang, and S.-T. Xia, “Periodicity decoupling framework for
626 long-term series forecasting,” in *International Conference on Learning Representations*, 2024.
627 [Online]. Available: <https://api.semanticscholar.org/CorpusID:271746144>
628
- 629 S. Li, X. Jin, Y. Xuan, X. Zhou, W. Chen, Y.-X. Wang, and X. Yan, “Enhancing the locality and
630 breaking the memory bottleneck of transformer on time series forecasting,” *Advances in neural
631 information processing systems*, vol. 32, 2019.
- 632 N. Wu, B. Green, X. Ben, and S. O’Banion, “Deep transformer models for time series forecasting:
633 The influenza prevalence case,” *arXiv preprint arXiv:2001.08317*, 2020.
- 634 B. Lim, S. Ö. Arık, N. Loeff, and T. Pfister, “Temporal fusion transformers for interpretable multi-
635 horizon time series forecasting,” *International Journal of Forecasting*, vol. 37, no. 4, pp. 1748–
636 1764, 2021.
- 637 Q. Wen, T. Zhou, C. Zhang, W. Chen, Z. Ma, J. Yan, and L. Sun, “Transformers in time series: A
638 survey,” *arXiv preprint arXiv:2202.07125*, 2022.
- 639 N. Kitaev, Ł. Kaiser, and A. Levskaya, “Reformer: The efficient transformer,” *arXiv preprint
640 arXiv:2001.04451*, 2020.
- 641 Q.-s. Zhang and S.-C. Zhu, “Visual interpretability for deep learning: a survey,” *Frontiers of Infor-
642 mation Technology & Electronic Engineering*, vol. 19, no. 1, pp. 27–39, 2018.
- 643
644
645
646
647

648 L. Shen and Y. Wang, “Tcct: Tightly-coupled convolutional transformer on time series forecasting,”
649 *Neurocomputing*, vol. 480, pp. 131–145, 2022.
650

651 K. Madhusudhanan, J. Burchert, N. Duong-Trung, S. Born, and L. Schmidt-Thieme, “Yformer:
652 U-net inspired transformer architecture for far horizon time series forecasting,” *arXiv preprint*
653 *arXiv:2110.08255*, 2021.

654 Y. Liu, H. Wu, J. Wang, and M. Long, “Non-stationary transformers: Exploring the stationarity in
655 time series forecasting,” in *Neural Information Processing Systems*, 2022. [Online]. Available:
656 <https://api.semanticscholar.org/CorpusID:252968420>
657

658 G. Woo, C. Liu, D. Sahoo, A. Kumar, and S. C. H. Hoi, “Etsformer: Exponential smoothing
659 transformers for time-series forecasting,” *ArXiv*, vol. abs/2202.01381, 2022. [Online]. Available:
660 <https://api.semanticscholar.org/CorpusID:246485702>

661 X. Wang, T. Zhou, Q. Wen, J. Gao, B. Ding, and R. Jin, “Card: Channel aligned
662 robust blend transformer for time series forecasting,” in *International Conference on Learning*
663 *Representations*, 2023. [Online]. Available: <https://api.semanticscholar.org/CorpusID:258832653>
664

665 T. Zhou, P. Niu, X. Wang, L. Sun, and R. Jin, “One fits all: Power general time series
666 analysis by pretrained lm,” in *Neural Information Processing Systems*, 2023. [Online]. Available:
667 <https://api.semanticscholar.org/CorpusID:258741419>

668 K. Hornik, M. B. Stinchcombe, and H. L. White, “Multilayer feedforward networks are
669 universal approximators,” *Neural Networks*, vol. 2, pp. 359–366, 1989. [Online]. Available:
670 <https://api.semanticscholar.org/CorpusID:2757547>
671
672
673
674
675
676
677
678
679
680
681
682
683
684
685
686
687
688
689
690
691
692
693
694
695
696
697
698
699
700
701

A DATA ARRANGEMENT

In this section, we present the data arrangement for the train set, validation set, and test set. We give the default arrangement in Table 1. In Table 2, we describe data rearrangement about ETTh1&2 and ETTm1&2 in Section 5.5. Note: n represents the total number of time steps and T is $30*24$.

Table 1: The default arrangement of data split.

Dataset	Train Set	Val Set	Test Set
Weather	D[:n*0.7]	D[n*0.7:n*0.8]	D[n*0.8:]
ETTh1&2	D[:T*12]	D[T*12:T*16]	D[T*16:T*20]
ETTh1&2	D[:T*12*4]	D[T*12*4:T*16*4]	D[T*16*4:T*20*4]
ILI	D[:n*0.6]	D[n*0.6:n*0.8]	D[n*0.8:]
ECL	D[:n*0.7]	D[n*0.7:n*0.8]	D[n*0.8:]
Traffic	D[:n*0.7]	D[n*0.7:n*0.8]	D[n*0.8:]

Table 2: The data rearrangement of ETTh1&2 and ETTm1&2.

Dataset	Train Set	Val Set	Test Set
ETTh1&2	D[T*2:T*16]	D[:T*2]	D[T*16:T*20]
ETTh1&2	D[T*1*4:T*16*4]	D[:T*1*4]	D[T*16*4:T*20*4]

B THE UAT FORMAT OF MRFNET

Here, we follow the proof process from UAT2LLMs and UAT2CVs to demonstrate that MRFNet is also a specific implementation of the UAT. We know the general format of MRFNet is:

$$\begin{aligned} \mathbf{x}'_{i+1} = & \mathbf{W}'_{i+1,1}\mathbf{x}'_i + \mathbf{b}'_{i+1,1} + \sigma(\mathbf{W}'_{i+1,2}\mathbf{x}'_i + \mathbf{b}'_{i+1,2}) \\ & + \sigma(\mathbf{W}'_{i+1,3}\mathbf{x}'_i + \mathbf{b}'_{i+1,3}) + \sigma(\mathbf{W}'_{i+1,4}\mathbf{x}'_i + \mathbf{b}'_{i+1,4}) \end{aligned} \quad (1)$$

According to UAT2LLMs and UAT2CVs, the general term of MRFNet is similar to the general term in UAT2LLMs(C.2) and UAT2CVs (A.2) by only two additional terms. According to these two UAT2LLMs and UAT2CVs, if the mathematical format of \mathbf{x}'_i is the same to UAT, then the mathematical format of $\mathbf{W}'_{i+1,1}\mathbf{x}'_i$ is also the same with UAT and $\sigma(\mathbf{W}'_{i+1,2}\mathbf{x}'_i + \mathbf{b}'_{i+1,2})$, $\sigma(\mathbf{W}'_{i+1,3}\mathbf{x}'_i + \mathbf{b}'_{i+1,3})$ and $\sigma(\mathbf{W}'_{i+1,4}\mathbf{x}'_i + \mathbf{b}'_{i+1,4})$ can be seen as three terms in UAT. So it is straightforward to deduce that if the mathematical form of \mathbf{x}'_i in MRFNet is consistent with the UAT form, then the mathematical form of \mathbf{x}'_{i+1} will also be consistent with the UAT form. It is also easy to derive that the mathematical forms of \mathbf{x}'_1 and \mathbf{x}'_2 in MRFNet are consistent with the UAT. Thus, by mathematical induction, the mathematical form of MRFNet aligns with the UAT.

For the clarity, we give the mathematical format of \mathbf{x}'_1 and \mathbf{x}'_2 , let the input to MRF Block 1 be \mathbf{x}_0 . Then, the matrix-vector form of \mathbf{x}'_1 can be expressed as shown in Eq. (2). Here, \mathbf{x}'_1 can be considered as being approximated by a UAT with N equal to 4.

$$\begin{aligned} \mathbf{x}'_1 = & \mathbf{W}'_{1,1}\mathbf{x}'_0 + \mathbf{b}'_{1,1} + \sigma(\mathbf{W}'_{1,2}\mathbf{x}'_0 + \mathbf{b}'_{1,2}) \\ & + \sigma(\mathbf{W}'_{1,3}\mathbf{x}'_0 + \mathbf{b}'_{1,3}) + \sigma(\mathbf{W}'_{1,4}\mathbf{x}'_0 + \mathbf{b}'_{1,4}) \end{aligned} \quad (2)$$

Similarly, based on Eq. (2), we can derive \mathbf{x}'_2 as shown in Eq. (3). Define the following: $\mathbf{W}'_{2,1} = \mathbf{W}'_{2,1}\mathbf{W}'_{1,1}$, $\mathbf{b}'_{2,1} = \mathbf{W}'_{2,1}\mathbf{b}'_{1,1} + \mathbf{b}'_{2,1}$, $\mathbf{W}'_{2,2} = \mathbf{W}'_{2,2}\mathbf{W}'_{1,1}$, $\mathbf{W}'_{2,3} = \mathbf{W}'_{2,3}\mathbf{W}'_{1,1}$, $\mathbf{W}'_{2,4} = \mathbf{W}'_{2,4}\mathbf{W}'_{1,1}$, $\mathbf{b}'_{2,2} = (\mathbf{W}'_{2,2}\mathbf{b}'_{1,1} + \mathbf{b}'_{2,2}) + \mathbf{W}'_{2,2}\sigma(\mathbf{W}'_{1,2}\mathbf{x}'_0 + \mathbf{b}'_{1,2}) + \mathbf{W}'_{2,2}\sigma(\mathbf{W}'_{1,3}\mathbf{x}'_0 + \mathbf{b}'_{1,3}) + \mathbf{W}'_{2,2}\sigma(\mathbf{W}'_{1,4}\mathbf{x}'_0 + \mathbf{b}'_{1,4})$, $\mathbf{b}'_{2,3} = (\mathbf{W}'_{2,3}\mathbf{b}'_{1,1} + \mathbf{b}'_{2,3}) + \mathbf{W}'_{2,3}\sigma(\mathbf{W}'_{1,2}\mathbf{x}'_0 + \mathbf{b}'_{1,2}) + \mathbf{W}'_{2,3}\sigma(\mathbf{W}'_{1,3}\mathbf{x}'_0 + \mathbf{b}'_{1,3}) + \mathbf{W}'_{2,3}\sigma(\mathbf{W}'_{1,4}\mathbf{x}'_0 + \mathbf{b}'_{1,4})$, and $\mathbf{b}'_{2,4} = (\mathbf{W}'_{2,4}\mathbf{b}'_{1,1} + \mathbf{b}'_{2,4}) + \mathbf{W}'_{2,4}\sigma(\mathbf{W}'_{1,2}\mathbf{x}'_0 + \mathbf{b}'_{1,2}) + \mathbf{W}'_{2,4}\sigma(\mathbf{W}'_{1,3}\mathbf{x}'_0 + \mathbf{b}'_{1,3}) + \mathbf{W}'_{2,4}\sigma(\mathbf{W}'_{1,4}\mathbf{x}'_0 + \mathbf{b}'_{1,4})$. Therefore, \mathbf{x}'_2 can be expressed as shown in Eq. (4), which can be seen as 7 layers' UAT. Thus, an MRFNet with i layers is equivalent to a UAT

with $3i + 1$ layers, effectively increasing the number of layers in the UAT. This is because, according to UAT2LLMs and UAT2CVs, a network with i layers generally corresponds to a UAT with $i + 1$ layers.

$$\begin{aligned}
\mathbf{x}'_2 &= \mathbf{W}'_{2,1}\mathbf{x}'_1 + \mathbf{b}'_{2,1} + \sigma(\mathbf{W}'_{2,2}\mathbf{x}'_1 + \mathbf{b}'_{1,2}) \\
&+ \sigma(\mathbf{W}'_{2,3}\mathbf{x}'_1 + \mathbf{b}'_{2,3}) + \sigma(\mathbf{W}'_{2,4}\mathbf{x}'_1 + \mathbf{b}'_{2,4}) \\
&= \mathbf{W}'_{2,1}[\mathbf{W}'_{1,1}\mathbf{x}'_0 + \mathbf{b}'_{1,1} + \sigma(\mathbf{W}'_{1,2}\mathbf{x}'_0 + \mathbf{b}'_{1,2}) + \sigma(\mathbf{W}'_{1,3}\mathbf{x}'_0 + \mathbf{b}'_{1,3}) \\
&+ \sigma(\mathbf{W}'_{1,4}\mathbf{x}'_0 + \mathbf{b}'_{1,4})] + \mathbf{b}'_{2,1} \\
&+ \sigma\{\mathbf{W}'_{2,2}[\mathbf{W}'_{1,1}\mathbf{x}'_0 + \mathbf{b}'_{1,1} + \sigma(\mathbf{W}'_{1,2}\mathbf{x}'_0 + \mathbf{b}'_{1,2}) + \sigma(\mathbf{W}'_{1,3}\mathbf{x}'_0 + \mathbf{b}'_{1,3}) \\
&+ \sigma(\mathbf{W}'_{1,4}\mathbf{x}'_0 + \mathbf{b}'_{1,4})] + \mathbf{b}'_{1,2}\} \\
&+ \sigma\{\mathbf{W}'_{2,3}[\mathbf{W}'_{1,1}\mathbf{x}'_0 + \mathbf{b}'_{1,1} + \sigma(\mathbf{W}'_{1,2}\mathbf{x}'_0 + \mathbf{b}'_{1,2}) + \sigma(\mathbf{W}'_{1,3}\mathbf{x}'_0 + \mathbf{b}'_{1,3}) \\
&+ \sigma(\mathbf{W}'_{1,4}\mathbf{x}'_0 + \mathbf{b}'_{1,4})] + \mathbf{b}'_{2,3}\} \\
&+ \sigma\{\mathbf{W}'_{2,4}[\mathbf{W}'_{1,1}\mathbf{x}'_0 + \mathbf{b}'_{1,1} + \sigma(\mathbf{W}'_{1,2}\mathbf{x}'_0 + \mathbf{b}'_{1,2}) + \sigma(\mathbf{W}'_{1,3}\mathbf{x}'_0 + \mathbf{b}'_{1,3}) \\
&+ \sigma(\mathbf{W}'_{1,4}\mathbf{x}'_0 + \mathbf{b}'_{1,4})] + \mathbf{b}'_{2,4}\} \\
&= (\mathbf{W}'_{2,1}\mathbf{W}'_{1,1}\mathbf{x}'_0 + \mathbf{W}'_{2,1}\mathbf{b}'_{1,1} + \mathbf{b}'_{2,1}) + \mathbf{W}'_{2,1}\sigma(\mathbf{W}'_{1,2}\mathbf{x}'_0 + \mathbf{b}'_{1,2}) + \mathbf{W}'_{2,1}\sigma(\mathbf{W}'_{1,3}\mathbf{x}'_0 + \mathbf{b}'_{1,3}) \\
&+ \mathbf{W}'_{2,1}\sigma(\mathbf{W}'_{1,4}\mathbf{x}'_0 + \mathbf{b}'_{1,4}) \\
&+ \sigma\{(\mathbf{W}'_{2,2}\mathbf{W}'_{1,1}\mathbf{x}'_0 + \mathbf{W}'_{2,2}\mathbf{b}'_{1,1} + \mathbf{b}'_{1,2}) + \mathbf{W}'_{2,2}\sigma(\mathbf{W}'_{1,2}\mathbf{x}'_0 + \mathbf{b}'_{1,2}) + \mathbf{W}'_{2,2}\sigma(\mathbf{W}'_{1,3}\mathbf{x}'_0 + \mathbf{b}'_{1,3}) \\
&+ \mathbf{W}'_{2,2}\sigma(\mathbf{W}'_{1,4}\mathbf{x}'_0 + \mathbf{b}'_{1,4})\} \\
&+ \sigma\{(\mathbf{W}'_{2,3}\mathbf{W}'_{1,1}\mathbf{x}'_0 + \mathbf{W}'_{2,3}\mathbf{b}'_{1,1} + \mathbf{b}'_{2,3}) + \mathbf{W}'_{2,3}\sigma(\mathbf{W}'_{1,2}\mathbf{x}'_0 + \mathbf{b}'_{1,2}) + \mathbf{W}'_{2,3}\sigma(\mathbf{W}'_{1,3}\mathbf{x}'_0 + \mathbf{b}'_{1,3}) \\
&+ \mathbf{W}'_{2,3}\sigma(\mathbf{W}'_{1,4}\mathbf{x}'_0 + \mathbf{b}'_{1,4})\} \\
&+ \sigma\{(\mathbf{W}'_{2,4}\mathbf{W}'_{1,1}\mathbf{x}'_0 + \mathbf{W}'_{2,4}\mathbf{b}'_{1,1} + \mathbf{b}'_{2,4}) + \mathbf{W}'_{2,4}\sigma(\mathbf{W}'_{1,2}\mathbf{x}'_0 + \mathbf{b}'_{1,2}) + \mathbf{W}'_{2,4}\sigma(\mathbf{W}'_{1,3}\mathbf{x}'_0 + \mathbf{b}'_{1,3}) \\
&+ \mathbf{W}'_{2,4}\sigma(\mathbf{W}'_{1,4}\mathbf{x}'_0 + \mathbf{b}'_{1,4})\}
\end{aligned} \tag{3}$$

$$\begin{aligned}
\mathbf{x}'_2 &= (\mathbf{W}'_{2,1}\mathbf{x}'_0 + \mathbf{b}'_{2,1}) + \mathbf{W}'_{2,1}\sigma(\mathbf{W}'_{1,2}\mathbf{x}'_0 + \mathbf{b}'_{1,2}) \\
&+ \mathbf{W}'_{2,1}\sigma(\mathbf{W}'_{1,3}\mathbf{x}'_0 + \mathbf{b}'_{1,3}) + \mathbf{W}'_{2,1}\sigma(\mathbf{W}'_{1,4}\mathbf{x}'_0 + \mathbf{b}'_{1,4}) \\
&+ \sigma(\mathbf{W}'_{2,2}\mathbf{x}'_0 + \mathbf{b}'_{2,2}) + \sigma(\mathbf{W}'_{2,3}\mathbf{x}'_0 + \mathbf{b}'_{2,3}) \\
&+ \sigma(\mathbf{W}'_{2,4}\mathbf{x}'_0 + \mathbf{b}'_{2,4})
\end{aligned} \tag{4}$$

C THE DATA PROBLEM OF ILI

Figure 1 illustrates the data trends for the 7 features in the ILI dataset, labeled as Class 1 to Class 7. Time series data generally exhibit two main characteristics: periodicity and trends within each period. The seven features share a similar period; however, it is evident that Classes 6 and 7 show an upward trend over time, while the overall trends of the other features remain stable.

If there is any correlation between the features, we believe it would be either related to the period (which is the same across features and can thus be disregarded) or to the trend. Since Classes 6 and 7 both display a rising trend, while the trends of the other classes remain unchanged, we hypothesize that Classes 6 and 7 should be separated from the other features. Therefore, we grouped the data into two sets: one containing Classes 6 and 7, and the other with the remaining features. We then trained and tested the model on these separate groups. The test results, shown in Table 3, clearly indicate a significant improvement in model performance after grouping the data for training.

D THE PROPERTIES OF FOURIER TRANSFORM

Compared to convolution, learning features in the Fourier domain offers the advantage of a larger receptive field. This phenomenon is illustrated in Figures 2 and 3. Figure 2 shows a typical convolu-

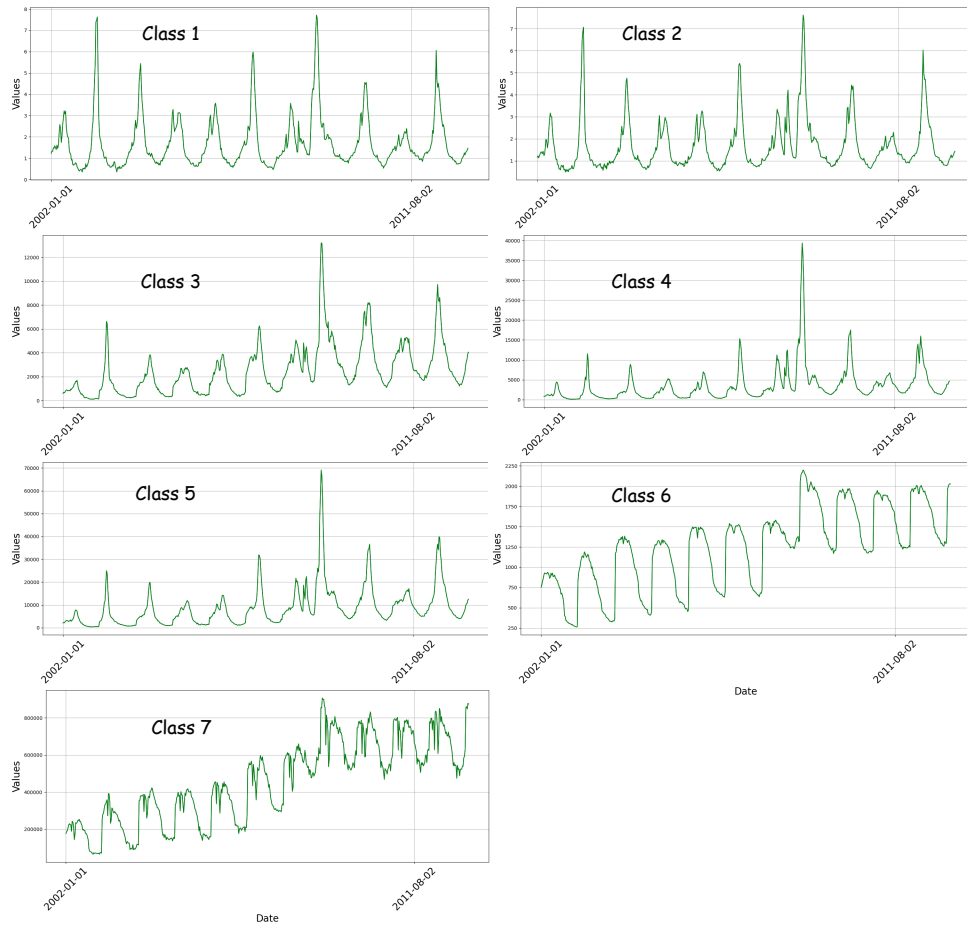


Figure 1: The trends of the features in the ILI dataset.

Table 3: Based on the characteristics of the ILI data, we divided it into two groups: Group 1: Class 1, 2, 3, 4, 5; Group 2: Class 6, 7. We then calculated the MSE and MAE for each group separately. Ori: Results from training with all features together. Split: Results from training after splitting the features into two groups.

Methods	Metric	Class 1		Class 2		Class 3		Class 4		Class 5		Class 6		Class 7	
		MSE	MAE	MSE	MAE	MSE	MAE								
Ori	24	0.532	0.764	0.602	0.987	1.085	2.527	0.968	2.501	1.196	3.635	0.736	0.821	0.876	1.062
	36	0.630	0.981	0.656	1.149	1.149	2.908	1.052	3.075	1.364	4.744	0.689	0.695	0.868	1.042
	48	0.596	0.891	0.644	1.063	1.129	2.801	1.035	2.867	1.266	4.356	0.727	0.763	0.892	1.063
	60	0.566	0.807	0.621	0.986	1.193	3.051	1.025	2.785	1.250	4.210	0.824	0.922	0.980	1.222
	Avg	0.581	0.860	0.630	1.046	1.139	2.821	1.020	2.807	1.269	4.236	0.744	0.800	0.904	1.097
Split	24	0.402	0.284	0.372	0.260	0.308	0.178	0.360	0.292	0.412	0.334	0.154	0.204	0.047	0.079
	36	0.350	0.217	0.326	0.206	0.289	0.160	0.275	0.146	0.343	0.210	0.182	0.060	0.221	0.091
	48	0.370	0.229	0.339	0.211	0.299	0.157	0.309	0.199	0.368	0.251	0.207	0.072	0.240	0.103
	60	0.342	0.205	0.320	0.206	0.281	0.147	0.275	0.159	0.345	0.222	0.211	0.076	0.231	0.103
	Avg	0.366	0.233	0.339	0.220	0.294	0.160	0.304	0.199	0.367	0.254	0.1885	0.103	0.184	0.094

tion process with a kernel size of 3, resulting in a receptive field of 3. In contrast, the black boxes of Figure 3 depict a standard Fourier transform process, while the right side (highlighted in the red box) demonstrates learning in the Fourier space based on the Fourier transform results from the left. It is evident that every point within the red box on the right is capable of gathering global information from the original domain, thus offering an expanded receptive field compared to convolution.

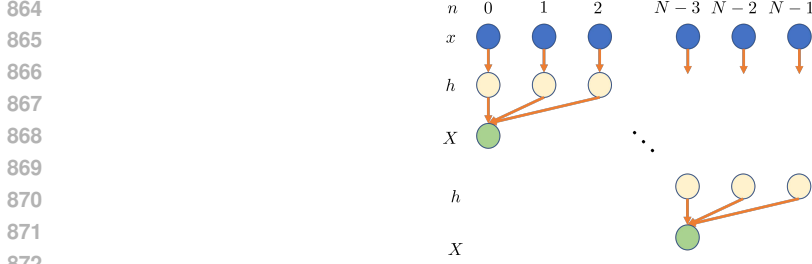


Figure 2: The convolution operation on the sequence. n is the serial number. \mathbf{x} is a sequence. \mathbf{h} is the convolutional kernel and the kernel size is three. \mathbf{X} is the output after convolution.

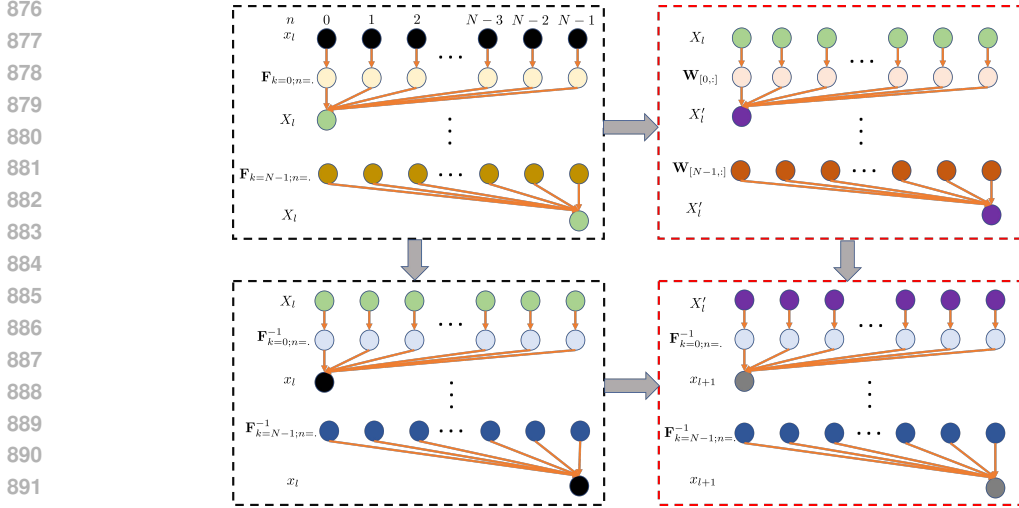


Figure 3: The left part is the Fourier transform. n is the serial number and $n = \cdot$ represents $n = 0, 1, 2, \dots$. \mathbf{x}_l and \mathbf{x}_{l+1} are latent sequences. \mathbf{F} is the FT matrix and \mathbf{F}^{-1} is inverse matrix of the FT. The right part is the way of learning the change of sequence in the Fourier domain. \mathbf{W} is the weight matrix. \mathbf{X}_l is the FT output. \mathbf{X}'_l is the latent features learned in the Fourier domain.

E VISUALIZATION OF WEIGHTS

Figures 4, 5, 6, and 7 illustrate the visual comparison of parameter weight information within the second MRF block of the MRFNet model on ETTh1 dataset, along with the weight information at corresponding positions for LS, LC, and LF. Overall, from the texture of these images, it can be observed that they learn similar information.

Linear Block: The overall texture learned by the Linear Block is similar, yet the weight parameter magnitudes differ among the models. Regarding the matrix multiplication, the x-axis corresponds to input time information, while the y-axis corresponds to output time information. In the row direction, there is an overall appearance of an interlocking grid pattern. This pattern signifies that different positions of input have varying degrees of importance for the output, and this importance changes continuously. Among these models, the LS model’s parameters exhibit this characteristic most prominently. This is primarily due to the LS model learning a sparse matrix, implying a block-wise learning of temporal information. Therefore, the linear Block complements this block-wise feature, reinforcing the coordination of local and global information. The other models learn information holistically, which is why this characteristic is less evident.

Sparse Matrix Block: The Sparse Matrix Block demonstrates a similar texture of weight features as the linear Block, with the distinction that this pattern is block-wise. The MRFNet model learns more discrete feature information, whereas the LS model learns continuous, block-wise information. However, the underlying patterns they learn are similar.

918
 919
 920
 921
 922
 923
 924
 925
 926
 927
 928
 929
 930
 931
 932
 933
 934
 935
 936
 937
 938
 939
 940
 941
 942
 943
 944
 945
 946
 947
 948
 949
 950
 951
 952
 953
 954
 955
 956
 957
 958
 959
 960
 961
 962
 963
 964
 965
 966
 967
 968
 969
 970
 971

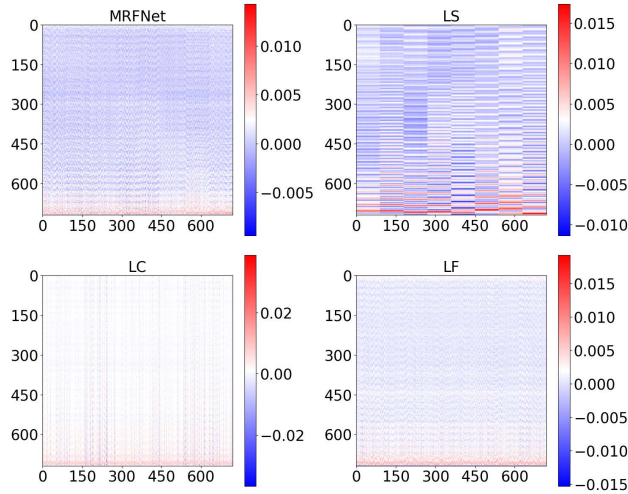


Figure 4: The images depict the weights of the Linear Block for the same layer corresponding to MRFNet, LS, LC, and LF.

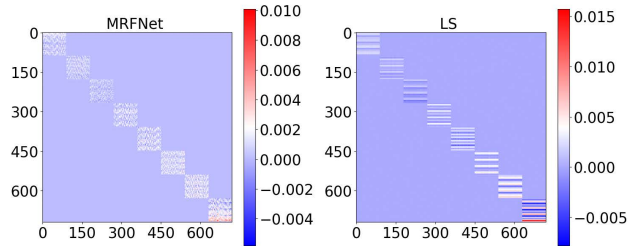


Figure 5: The images depict the weights of the Sparse Matrix Block for the same layer corresponding to MRFNet and LS.

Convolutional Block: Given a kernel size of 3, the display of convolutional kernel weights is organized according to the kernel positions. It is evident that the textures they learn are highly alike.

FT Block: The FT Block’s weights consist of real and imaginary components, each displayed separately. The similarity of the textures is conspicuous.

In summary, the weights corresponding to LS, LC, and LF in the MRFNet model are notably similar. This observation indicates that they collectively learn akin information, which is coherent due to being trained on the same dataset. Additionally, as the MRFNet model comprises multiple modules, these modules function complementarily. Consequently, specific differences emerge among these modules.

F PROFERMANCES OF UNIVARIATE PREDICTION

We compared preferences for univariate prediction in Table 4. Overall, our results are similar to the PatchTST and outperform other models.

G THE PREDICTION RESULTS OF MRFNET

Figure 8 presents the prediction results of the HUFL feature in the ETTm1 dataset. As shown in the figure, our model outperforms the PatchTST, DLinear, and Autoformer models.

972
 973
 974
 975
 976
 977
 978
 979
 980
 981
 982
 983
 984
 985
 986
 987
 988
 989
 990
 991
 992
 993
 994
 995
 996
 997
 998
 999
 1000
 1001
 1002
 1003
 1004
 1005
 1006
 1007
 1008
 1009
 1010
 1011
 1012
 1013
 1014
 1015
 1016
 1017
 1018
 1019
 1020
 1021
 1022
 1023
 1024
 1025

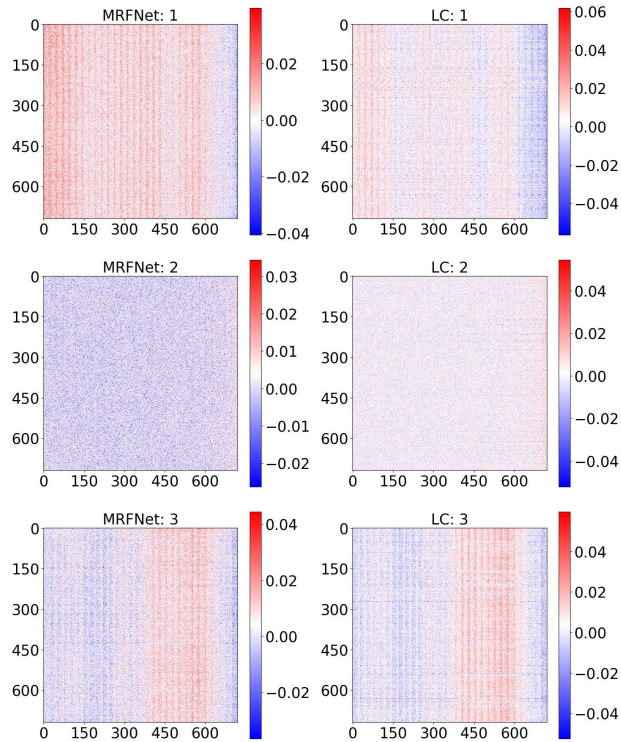


Figure 6: The images depict the weights of the Conv Block for the same layer corresponding to MRFNet and LC. The input and output dimensions are 720 and the kernel size is three, so the dimensions of the kernel are $(720, 720, 3)$. In this figure, 1, 2, and 3 denote the number of the third dimension direction of $(720, 720, 3)$.

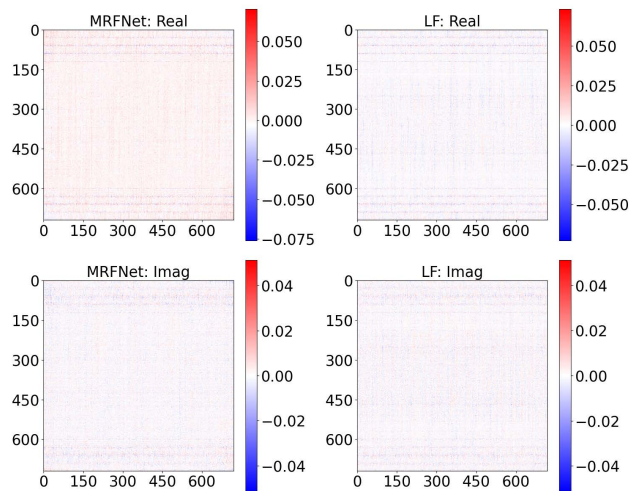


Figure 7: The images depict the weights of the Fourier Block for the same layer corresponding to MRFNet and LF. Real and Imag represent the real and imaginary parts of the weights in Fourier domain.

1026
1027
1028
1029
1030
1031
1032
1033
1034
1035
1036
1037
1038
1039
1040
1041
1042
1043
1044
1045
1046
1047
1048
1049
1050
1051
1052
1053
1054
1055
1056
1057
1058
1059
1060
1061
1062
1063
1064
1065
1066
1067
1068
1069
1070
1071
1072
1073
1074
1075
1076
1077
1078
1079

Table 4: Univariate predictions of ETTh1, ETTh2, ETTm1, and ETTm2 by twelve models.

Models	MRFNet		PatchTST/64		DLinear		FEDformer		Autoformer		Informer		LogTrans		
	Metric	MSE	MAE	MSE	MAE	MSE	MAE	MSE	MAE	MSE	MAE	MSE	MAE	MSE	MAE
ETTh1	96	0.055	0.181	0.059	0.189	0.056	0.180	0.079	0.215	0.071	0.206	0.193	0.377	0.283	0.468
	192	0.071	0.206	0.074	0.215	0.071	0.204	0.104	0.245	0.114	0.262	0.217	0.395	0.234	0.409
	336	0.084	0.231	0.076	0.220	0.098	0.244	0.119	0.270	0.107	0.258	0.202	0.381	0.386	0.546
	720	0.098	0.246	0.087	0.236	0.189	0.359	0.142	0.299	0.126	0.283	0.183	0.355	0.475	0.629
ETTh2	96	0.151	0.301	0.131	0.284	0.131	0.279	0.128	0.271	0.153	0.306	0.213	0.373	0.217	0.379
	192	0.171	0.329	0.171	0.329	0.176	0.329	0.185	0.330	0.204	0.351	0.227	0.387	0.281	0.429
	336	0.186	0.345	0.171	0.336	0.209	0.367	0.231	0.378	0.246	0.389	0.242	0.401	0.293	0.437
	720	0.214	0.368	0.223	0.380	0.276	0.426	0.278	0.420	0.268	0.409	0.291	0.439	0.218	0.387
ETTm1	96	0.026	0.121	0.026	0.123	0.028	0.123	0.033	0.140	0.056	0.183	0.109	0.277	0.049	0.171
	192	0.041	0.153	0.040	0.151	0.045	0.156	0.058	0.186	0.081	0.216	0.151	0.310	0.157	0.317
	336	0.055	0.178	0.053	0.174	0.061	0.182	0.084	0.231	0.076	0.218	0.427	0.591	0.289	0.459
	720	0.070	0.203	0.073	0.206	0.080	0.210	0.102	0.250	0.110	0.267	0.438	0.586	0.430	0.579
ETTm2	96	0.063	0.181	0.065	0.187	0.063	0.183	0.067	0.198	0.065	0.189	0.088	0.225	0.075	0.208
	192	0.091	0.226	0.093	0.231	0.092	0.227	0.102	0.245	0.118	0.256	0.132	0.283	0.129	0.275
	336	0.128	0.272	0.121	0.266	0.119	0.261	0.130	0.279	0.154	0.305	0.180	0.336	0.154	0.302
	720	0.165	0.315	0.172	0.322	0.175	0.320	0.178	0.325	0.182	0.335	0.300	0.435	0.160	0.321

Table 5: Multivariate predictions of ETTh1, ETTh2, ETTm1, ETTm2, Traffic, Electricity, Weather and ILI, by twelve models. The best results are highlighted in bold red. The second-best results are indicated with highlighted in bold black.

Methods	MRFNet		GPT2(6)		DLinear		PatchTST		TimesNet		FEDformer		Autoformer		Stationary		ETSformer		LightTS		Informer		Reformer		
	Metric	MSE	MAE	MSE	MAE	MSE	MAE	MSE	MAE	MSE	MAE	MSE	MAE	MSE	MAE	MSE	MAE	MSE	MAE	MSE	MAE	MSE	MAE	MSE	MAE
Weather	96	0.149	0.191	0.162	0.212	0.176	0.237	0.149	0.198	0.172	0.220	0.217	0.296	0.266	0.336	0.173	0.223	0.197	0.281	0.182	0.242	0.300	0.384	0.689	0.596
	192	0.193	0.235	0.204	0.248	0.220	0.282	0.194	0.241	0.219	0.261	0.276	0.336	0.307	0.367	0.245	0.285	0.237	0.312	0.227	0.287	0.598	0.544	0.752	0.638
	336	0.245	0.278	0.254	0.286	0.265	0.319	0.245	0.282	0.280	0.306	0.339	0.380	0.359	0.395	0.321	0.338	0.298	0.353	0.282	0.334	0.578	0.523	0.639	0.596
	720	0.315	0.329	0.326	0.337	0.333	0.362	0.314	0.334	0.365	0.359	0.403	0.428	0.419	0.428	0.414	0.410	0.352	0.288	0.352	0.386	1.059	0.741	1.130	0.792
	Avg	0.225	0.258	0.237	0.270	0.248	0.300	0.225	0.264	0.259	0.287	0.309	0.360	0.338	0.382	0.288	0.314	0.271	0.334	0.261	0.312	0.634	0.548	0.803	0.656
ETTh1	96	0.364	0.393	0.376	0.397	0.375	0.399	0.370	0.399	0.384	0.402	0.376	0.419	0.449	0.459	0.513	0.491	0.494	0.479	0.424	0.432	0.865	0.713	0.837	0.728
	192	0.402	0.415	0.416	0.418	0.405	0.416	0.413	0.421	0.436	0.429	0.420	0.448	0.500	0.482	0.534	0.504	0.538	0.504	0.475	0.462	1.008	0.792	0.923	0.766
	336	0.442	0.444	0.442	0.433	0.439	0.443	0.422	0.436	0.491	0.469	0.459	0.465	0.521	0.496	0.588	0.535	0.574	0.521	0.518	0.488	1.107	0.809	1.097	0.835
	720	0.434	0.454	0.477	0.456	0.472	0.490	0.447	0.466	0.521	0.500	0.506	0.507	0.514	0.512	0.643	0.616	0.562	0.535	0.547	0.533	1.181	0.865	1.257	0.889
	Avg	0.410	0.426	0.427	0.426	0.422	0.437	0.413	0.430	0.458	0.450	0.440	0.460	0.496	0.487	0.570	0.537	0.542	0.510	0.491	0.479	1.040	0.795	1.029	0.805
ETTh2	96	0.273	0.330	0.285	0.342	0.289	0.353	0.274	0.336	0.340	0.374	0.358	0.397	0.346	0.388	0.476	0.458	0.340	0.391	0.397	0.437	3.755	1.525	2.626	1.317
	192	0.341	0.376	0.354	0.389	0.383	0.418	0.339	0.379	0.402	0.414	0.429	0.439	0.456	0.452	0.512	0.493	0.430	0.439	0.520	0.504	5.602	1.931	11.12	2.979
	336	0.366	0.396	0.373	0.407	0.448	0.465	0.329	0.380	0.452	0.452	0.486	0.487	0.482	0.486	0.552	0.551	0.485	0.479	0.626	0.559	4.721	1.835	9.323	2.769
	720	0.385	0.423	0.406	0.441	0.605	0.551	0.379	0.422	0.462	0.468	0.463	0.474	0.515	0.511	0.562	0.560	0.500	0.497	0.863	0.672	3.647	1.625	3.874	1.697
	Avg	0.341	0.381	0.354	0.394	0.431	0.446	0.330	0.379	0.414	0.427	0.437	0.449	0.450	0.459	0.526	0.516	0.439	0.452	0.602	0.543	4.431	1.729	6.736	2.191
ETTm1	96	0.297	0.342	0.292	0.346	0.299	0.343	0.290	0.342	0.338	0.375	0.379	0.419	0.505	0.475	0.386	0.398	0.375	0.398	0.374	0.400	0.672	0.571	0.538	0.528
	192	0.334	0.366	0.332	0.372	0.335	0.365	0.332	0.369	0.374	0.387	0.426	0.441	0.553	0.496	0.459	0.444	0.408	0.410	0.400	0.407	0.795	0.669	0.658	0.592
	336	0.366	0.385	0.366	0.394	0.369	0.386	0.366	0.392	0.410	0.411	0.445	0.459	0.621	0.537	0.495	0.464	0.435	0.428	0.438	0.438	1.212	0.871	0.898	0.721
	720	0.407	0.411	0.417	0.421	0.425	0.421	0.416	0.420	0.478	0.450	0.543	0.490	0.671	0.561	0.585	0.516	0.499	0.462	0.527	0.502	1.166	0.823	1.102	0.841
	Avg	0.351	0.376	0.352	0.383	0.357	0.378	0.351	0.380	0.400	0.406	0.448	0.452	0.588	0.517	0.481	0.456	0.429	0.425	0.435	0.437	0.961	0.734	0.799	0.671
ETTm2	96	0.163	0.246	0.173	0.262	0.167	0.269	0.165	0.255	0.187	0.267	0.203	0.287	0.255	0.339	0.192	0.274	0.189	0.280	0.209	0.308	0.365	0.453	0.658	0.619
	192	0.219	0.287	0.229	0.301	0.224	0.303	0.220	0.292	0.249	0.309	0.269	0.328	0.281	0.340	0.280	0.339	0.253	0.319	0.311	0.382	0.533	0.563	1.078	0.827
	336	0.275	0.323	0.286	0.341	0.281	0.342	0.274	0.329	0.321	0.351	0.325	0.366	0.339	0.372	0.334	0.361	0.314	0.357	0.442	0.466	1.363	0.887	1.549	0.972
	720	0.354	0.377	0.378	0.401	0.397	0.421	0.362	0.385	0.408	0.403	0.421	0.415	0.433	0.432	0.417	0.413	0.414	0.413	0.675	0.587	3.379	1.338	2.631	1.242
	Avg	0.252	0.333	0.266	0.326	0.267	0.333	0.255	0.315	0.291	0.333	0.305	0.349	0.327	0.371	0.306	0.347	0.293	0.342	0.409	0.436	1.410	0.810	1.479	0.915
ILI	24	1.757	0.857	2.063	0.881	2.215	1.081	1.319	0.754	2.317	0.934	3.228	1.260	3.483	1.287	2.294	0.945	2.527	1.020	8.313	2.144	5.764	1.677	4.400	1.382
	36	2.085	0.915	1.868	0.892	1.963	0.963	1.430	0.834	1.972	0.920	2.679	1.080	3.103	1.148	1.825	0.848	2.615	1.007	6.631	1.902	4.755	1.467	4.783	1.448
	48	1.972	0.899	1.790	0.884	2.130	1.024	1.553	0.815	2.238	0.940	2.622	1.078	2.669	1.085	2.010	0.900	2.359	0.972	7.299	1.982	4.763	1.469	4.832	1.465
	60	1.998	0.923	1.979	0.957	2.368	1.096	1.470	0.788	2.027	0.928	2.857													

1080
1081
1082
1083
1084
1085
1086
1087
1088
1089
1090
1091
1092
1093
1094
1095
1096
1097
1098
1099
1100
1101
1102
1103
1104
1105
1106
1107
1108
1109
1110
1111
1112
1113
1114
1115
1116
1117
1118
1119
1120
1121
1122
1123
1124
1125
1126
1127
1128
1129
1130
1131
1132
1133

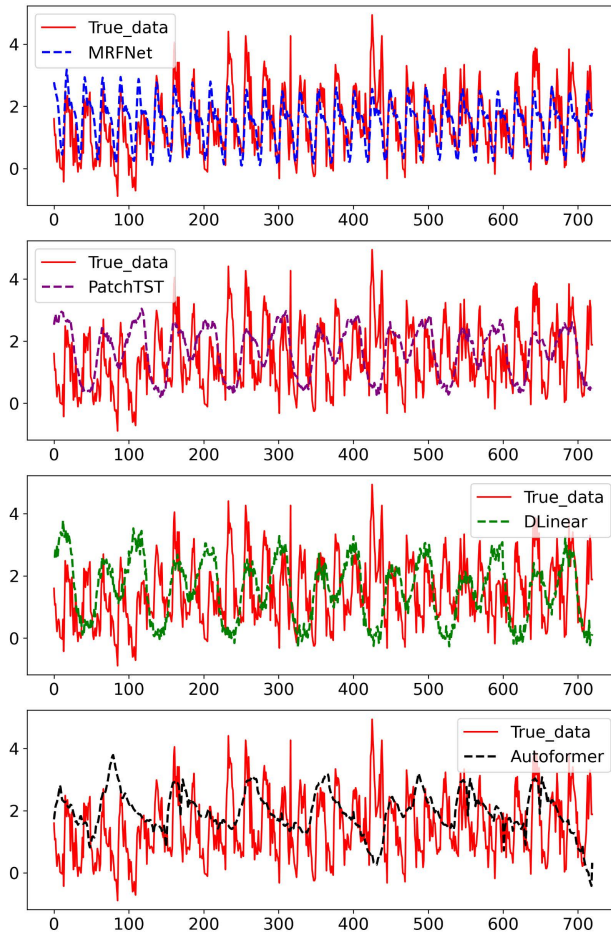


Figure 8: The prediction results (Horizon = 720; HUFL) of MRFNet, PatchTST, DLinear, Autoformer on the ETTm1 dataset.